Clusters in colloidal dispersions with a short-range depletion attraction: Thermodynamic identification and morphology

Clusters in colloidal dispersions with a short-range depletion attraction: thermodynamic identification and morphology

Fernando Soto-Bustamante[a,b], Néstor E. Valadez-Pérez[c], Yun Liu[d,e], Ramón Castañeda-Priego[a], Marco Laurati[b*]

[a] *División de Ciencias e Ingenierías, Campus León, Universidad de Guanajuato, Loma del Bosque 103, Lomas del Campestre, 37150 León, Guanajuato, Mexico*

[b] *Dipartimento di Chimica & CSGI, Università di Firenze, 50019 Sesto Fiorentino, Italy*

[c] *Facultad de Ciencias en Física y Matemáticas, Universidad Autónoma de Chiapas, Carretera Emiliano Zapata km 8, 29050, Tuxtla Gutiérrez, Chiapas, Mexico*

[d] *NIST Center for Neutron Research, National Institute of Standards and Technology, 20899 Gaithersburg, Maryland, United States*

[e] *Department of Chemical and Biomolecular Engineering, University of Delaware, 19716 Newark, Delaware, United States*

Abstract

Hypothesis: Particle aggregation is ubiquitous for many colloidal systems, and drives the phase separation or the formation of materials with a highly heterogeneous large-scale structure, such as gels, porous media and attractive glasses. While the macroscopic properties of such materials strongly depend on the shape and size of these particle aggregates, the morphology and underlining aggregation physical mechanisms are far from being fully understood. Recently, it has been proposed that for reversible colloidal aggregation, the cluster morphology in the case of colloids interacting with short-range attractive forces is determined by a single variable, namely, the reduced second virial coefficient, B_2^*.

Experiments: We examined this proposal by performing confocal microscopy experiments and computer simulations on a large collection of short-ranged attractive colloidal systems with different values of the attraction strength and range.

Findings: We show that in all cases a connection between the colloidal cluster morphology and B_2^* can be established both in experiments and simulations. This physical scenario holds at all investigated thermodynamic conditions, namely, in the fluid state, in the metastable region and in non-equilibrium conditions. Our findings support the connection between reversible colloidal aggregation and the so-called extended law of corresponding states.

*Corresponding author

Email address: marco.laurati@unifi.it (Marco Laurati[b])

Keywords: Colloidal aggregation, clusters, fractal dimension, extended law of corresponding states

1. Introduction

Colloidal dispersions are commonly encountered in our everyday life and can exist as equilibrium phases, for instance liquids and crystals [1, 2], or non-equilibrium states, such as gels and glasses [2, 3, 4]. These dispersions have important industrial applications (in paints, drugs, food, etc.) [5, 6, 7, 8], and serve as very useful testbeds to investigate fundamental physical phenomena that are hardly accessible in experiments on atomic and molecular systems [9, 10].

Cluster formation in colloidal dispersions plays important roles to determine their macroscopic properties and has been studied under both equilibrium and non-equilibrium conditions. [11, 4, 12, 13, 14, 15, 11, 16]. The formation of equilibrium clusters in fluids can cause some interesting rheological properties [17], which can be associated to unique structures of clusters [16]. According to Ref. [18], the formation of mechanically stable rigid clusters is associated to the physical mechanism that controls colloidal gelation. Clustering is also a preliminary step that leads to the transition to different phases with large scale heterogeneous structures, such as those observed at the gas-liquid phase separation, during the nucleation process of a colloidal crystal and at gelation [2, 14, 12, 13, 19, 20]. Clustering has been studied in colloidal systems interacting with different inter-particle potentials and under different thermodynamic conditions, see, e.g., Ref. [21] and references therein. Experiments have shown that colloidal clusters have a fractal structure [22, 4, 11, 15, 23, 12], i.e., the mass of a cluster grows as $m \sim l^{d_f}$, where l is a characteristic length and d_f is the so-called fractal dimension. Compact structures have a large fractal dimension $d_f \sim 2.5$, or larger, while ramified or branched clusters a $d_f \sim 1.5$ [11, 12, 15].

For colloids interacting with a short-range depletion attraction, Poon et al. [22] related the cluster morphology to the strength of the depletion attraction, while Lu et al. [11] claimed that the attraction range determines the fractal dimension of clusters in the vicinity of the gel transition. While long ranged attractions lead to compact clusters, small ranged attractions produce open and branched structures. Furthermore, Sánchez and Bartlett [24] showed that the particle concentration also modifies the cluster morphology when a small amount of charge is additionally present. Clusters at concentrations below the critical gel formation have a fractal dimension close to the one observed in the irreversible process known as diffusion-limited cluster aggregation (DLCA), $d_f \sim 1.8$, while clusters in the gel state have a fractal dimension similar to the irreversible mechanism called reaction-limited cluster aggregation (RCLA), $d_f \sim 2.1$ [25]. Additionally, Ohtsuka et al. [12] found that the attraction strength modifies d_f and that the fractal dimension reaches an almost constant value in the gel state, $d_f \sim 2.1$. However, none of the previous experimental studies have clearly elucidated the connection between the cluster morphology, the strength and range of the interparticle potential and the thermodynamic states of the dispersion. As cluster properties determine the dynamical and mechanical features of bulk colloidal fluids, it is thus important to understand particle aggregation under both equilibrium and non-equilibrium

conditions.

The law of corresponding states establishes that, although the molecular details of two distinct systems are different, their thermodynamic properties are basically the same when they are expressed in terms of the critical values [26]. Noro and Frenkel extended this empirical law to systems whose constituents interact with different short-ranged attractive potentials (the attraction range is less than the 25% of the particle diameter) [27]. They found that the thermodynamic properties of these systems are the same when they have the same: reduced density, $\rho^* \equiv \rho\sigma_{\rm eff}^3$, and reduced second virial coefficient, $B_2^* \equiv B_2/B_2^{\rm HS}$, where $B_2^{\rm HS} = 2\pi\sigma_{\rm eff}^3/3$ is the second virial coefficient of hard-spheres with the diameter $\sigma_{\rm eff}$. The Noro-Frenkel law of corresponding states was preceded by the so-called Vliegenthart-Lekkerkerker (VLc) criterion, which states that $B_2^* = -1.5$ at the critical point [28]. A few years ago, some of us tested this criterion [29] and found that this value depends slightly on the attraction range, however, the VLc provides a good estimate of the onset of the phase separation.

Recently, some of us proposed to establish a link between the cluster morphology in short-ranged attractive colloidal systems and the extended law of corresponding states [30]. Using Monte Carlo (MC) simulations of a square-well fluid, the effect of the potential features on the cluster morphology was studied. Two striking and novel features were found: colloids aggregate into small clusters, whose fractal dimension $d_{\rm f} \sim 1.8$ does not depend on the details of the attraction; and for large clusters, their morphology depends exclusively on B_2^*, i.e. $d_{\rm f}$ of large aggregates follows a master curve which is only a function of the reduced second virial coefficient. While the simulation results were compared with experimental data from the literature (Refs. [11, 12]), these data were not designed to fully examine the previous simulation findings. And, in particular, there were no studies about the cluster morphology in the meta-stable region and non-equilibrium gel states. In this contribution, we provide a comprehensive experimental data using a widely studied model system, namely, a colloid-polymer mixture [31]. In the limit of short-range attractions, i.e. when the range of the attraction is smaller than 15% of the particle diameter [32], the mixture can be considered as a single component system in which the effective attraction between colloidal particles is mediated by the polymers [33]. The strength of the attraction is determined by the polymer concentration and its range is given by the size ratio $\xi = 2r_{\rm g}/\sigma_{\rm c}$ [33, 34], where $r_{\rm g}$ is the radius of gyration of the polymers and $\sigma_{\rm c}$ is the colloidal particle diameter. Through this systematical study, we confirm the connection between cluster morphology and the extended law of corresponding states, showing that for the colloid-polymer mixtures of this work, the fractal dimension of both small and large clusters is a function of the quantity $c_{\rm p}/c_{\rm p}^*$, where $c_{\rm p}$ is the polymer mass concentration (w/v) and $c_{\rm p}^* = 3{\rm M_w}/(4\pi{\rm N_A}r_{\rm g}^3)$ the overlap concentration. Indeed, in the limit of small polymer-colloid size ratio $\xi = r_{\rm g}/R$, Free-Volume Theory predicts that the reduced second virial coefficient B_2^* is uniquely related to $c_{\rm p}/c_{\rm p}^*$ [35]. The relation between B_2^* and $c_{\rm p}/c_{\rm p}^*$ was also pointed out in recent work [30]. We complement the experimental findings with simulations of colloidal dispersions interacting through the Asakura-Oosawa potential, i.e., a potential that is expected to better model the experimental interactions than the square-well potential used in previous work.

System	M_w [g·mol$^-$1]	r_g [μm]	ξ	ξ (free)
1	3.00×10^6	0.0636	0.075	0.078
2	1.01×10^6	0.0333	0.039	0.042
3	8.64×10^5	0.0305	0.036	0.038
4	4.51×10^5	0.0211	0.025	0.026
5	1.01×10^5	0.0093	0.011	0.012

Table 1: Molecular weight, radius of gyration, r_g, and polymer-colloid size ratio ξ (nominal value) for the samples investigated in this work. The value ξ^{free} represents the polymer-colloid size ratio corrected according to the free volume of the samples.

2. Materials and Methods

2.1. Sample preparation

We experimentally studied mixtures of Polymethylmethacrylate (PMMA) hard sphere-like particles and non-adsorbing polystyrene (PS) chains dispersed in a solvent composed of cis-trans decahydronaphtalene and bromocycloheptane (CHB) that matches the density of the PMMA particles. The particles are sterically stabilized by a layer of grafted polyhydroxystearic acid (PHSA). Their average diameter is σ_c = 1.7 μm with a polydispersity of about 7%, as determined by dynamic light scattering (DLS). The particles are fluorescently labeled with nitrobenzoxadyazole (NBD). PS chains with molecular weight $M_w = 3 \times 10^6$ g/mol, 1.01×10^6 g/mol, 8.64×10^5 g/mol, 4.51×10^5 g/mol, 1.01×10^5 g/mol were used. The corresponding radius of gyration r_g was obtained using the following empirical relation which has been determined by DLS measurements of dilute solutions of PS in cis-decalin[36]:

$$r_g = r_g^\theta \sqrt{1 + \frac{134}{105} z(T)}, \tag{1}$$

where $r_g^\theta = 0.0276\sqrt{M_w}$ is the radius of gyration at the θ temperature T_θ and $z(T)$ is the Fixman parameter[36]:

$$z(T) = 0.00975\sqrt{M_w}\left(1 - \frac{T_\theta}{T}\right). \tag{2}$$

We have neglected any small swelling effect induced by the presence of CHB in addition to decalin in our samples. Values of r_g and of the polymer colloid size-ratio $\xi = 2r_g/\sigma_c$ for the different polymers used are reported in Table 1. The suspensions present a certain degree of charging. For similar suspensions, inverse screening lengths κ^{-1} comparable to the particle size (1-2 μm) have been reported [37, 38, 39], corresponding to a long-range electrostatic repulsion. However, suspensions without polymers investigated in this work were crystallizing into FCC lattices at the volume fraction, $\phi \approx 0.47$, indicating weak electrostatic contributions [38].

After mixing, samples were homogeneized in a rotating wheel for one day before measuring.

2.2. Confocal microscopy experiments

Confocal microscopy experiments were performed using a VT-Eye confocal unit (Visitech) mounted on a Nikon Ti-S inverted microscope. A 100x Plan-Apo oil-immersion objective with numerical aperture NA = 1.40 was used for all measurements. For each sample 50 stacks of 151 images of 512×512 pixels, corresponding to a volume of $58 \times 58 \times 30$ μm^3, were acquired at different locations in the sample and at a distance of 10μm from the coverslip in order to investigate the bulk structure of the mixtures. Particle coordinates were extracted from the measured stacks by using standard particle tracking routines [40].

From the particle coordinates, the formation of particle-particle bonds was determined according to the criterion that two particles are bonded when they lie at a distance smaller than $2R + 2r_g$. Once clusters of size s were identified according to this criterion, the cluster radius of gyration was calculated as [41]:

$$R_g(s) = \left[\frac{1}{s} \sum_{i=1}^{s} (r_i - r_{CM})^2 \right]^{1/2} \tag{3}$$

where r_i is the coordinate of particle i within the cluster and r_{CM} is the position of the center of mass of the cluster.

2.3. Cutoff distance and criteria for the distinction between compact and elongated clusters

We consider that two colloids form a bond when the separation between their surfaces is smaller than ξ [42]. Thus, $r_c = \xi$ is chosen here as the cutoff distance to distinguish the formation of bonds. Furthermore, the classification of clusters into compact or elongated, reported in Fig. 2, was performed by analyzing the bond probability distributions reported in Fig. S1 (see Supplementary Information). The average number of neighbors $\langle n \rangle$ was extracted from the distributions as a function of c_p/c_p^* and is reported in Fig. S2 for the different size ratios. Then, as explicitly discussed in the Supplementary Information, clusters were considered as compact when $\langle n \rangle > 4.5$, and elongated otherwise (see dashed line in Fig. S2).

2.4. Monte Carlo computer simulations

We have performed Monte Carlo computer simulations in the canonical ensemble for a colloidal system with 8000 particles and polydispersity of 7% (reflecting the polydispersity of the experimental system). Particles interact through the Asakura-Oosawa potential (4) [33]. The latter can be written as:

$$\frac{u(r)}{k_B T} = -\frac{\phi_p^{(R)}}{\xi^3} \left((1+\xi)^3 - \frac{3}{2}(1+\xi)^2 \frac{r}{\sigma_c} + \frac{r^3}{2\sigma_c^3} \right) \tag{4}$$

where k_B is the Boltzmann constant, T is the absolute temperature, $\phi_p^{(R)}$ is the polymer packing fraction in the free volume of the sample, see Ref. [2] and ξ is the depletion thickness. The latter is commonly taken as the size ratio $\xi = 2r_g/\sigma_c$, being r_g the radius of gyration of the polymer and σ_c is the colloid diameter. This potential is a

good representation of the effective interaction between colloids in the ideal case when polymers are sufficiently smaller than the colloidal particles, i.e., when $\xi \leq 0.1547$ [43], and when the colloidal density and polymer concentration are sufficiently small [44]. For a more accurate description of the depletion potential, we have used the correction to the depletion thickness from the renormalization group as used in Ref. [45], see Table 1. To calculate the gas-liquid coexistence, the simulations were set at $\phi_c = 0.2$ and the starting configuration was obtained from previous simulations with a hard sphere potential. A simulation run consisted of about 5×10^8 MC steps for different values of ϕ_p to reach equilibrium configurations. After this stage, in which the energy per particle presents small variations over several millions of MC steps, the local density was determined in a second stage of 5×10^7 MC steps. The density distribution displays an approximately Gaussian shape, centered on the bulk density, for states out of the phase coexistence but inside this region, the single peak splits in two peaks, which are used to estimate the density of the coexisting phases (data not shown). The results of these calculations were used to construct the binodal lines reported in Fig. S3. From this protocol, we estimated the binodal at $\phi_c = 0.1$ for all the experimentally explored colloidal systems with different ξ-values, see Fig 2. Note that in this figure, we use $c_p/c_p^* = \phi_p$; the latter expression is related with the parameter $\phi_p^{(R)}$ (see Eq. (4)), where $\phi_p = \alpha \phi_p^{(R)}$ and $\alpha(\xi, \phi_c)$ is known as the free volume fraction [45].

2.5. Polymer Critical Volume Fraction from Free Volume Theory

Free Volume Theory (FVT) [45, 46, 47, 48] provides a realistic approach to describe depletion interactions, taking into account the finite volume of polymers, the excluded volume due to the hard-sphere interaction between polymers and colloids, the fact that the depletion layer depends on the colloid size and also the polydispersity of both colloids and polymers [44]. The calculation of the phase equilibrium requires to calculate the thermodynamic properties, such as pressure and chemical potential, which are obtained from the free energy in the semi-grand canonical ensemble [45]. In this ensemble, the free energy is made up of two contributions: the first one comes from the colloids and the second from polymers. Then, this approach allows one to calculate the gas-liquid as well as the fluid-crystal phase separation by changing the expression for the colloids free energy. Here we use the FVT to calculate the fluid-crystal coexistence boundary for a qualitative comparison with the polymer critical volume fraction obtained from simulations, ϕ_p^c, see Fig S3. FVT provides also a way to estimate the second virial coefficient in experiments. According to Tuinier and coworkers [35], B_2^* in the limit of moderate colloid volume fractions can be written as:

$$B_2^* = B_2/B_2^{\mathrm{HS}} = 1 - \frac{1}{4}\frac{c_p}{c_p^*}\left[6 + \frac{15}{2}\xi + 3\xi^2 + \frac{1}{2}\xi^3\right]. \tag{5}$$

One should notice that in the limit $\xi \to 0$, i.e., for small size ratios, the reduced second virial coefficient is only a function of c_p/c_p^*. Therefore, Eq. 5 provides a direct link between B_2^* and c_p/c_p^*. This is also a result consistent with theoretical findings provided by the so-called PRISM theory [49]. If one considers the previous equation along with

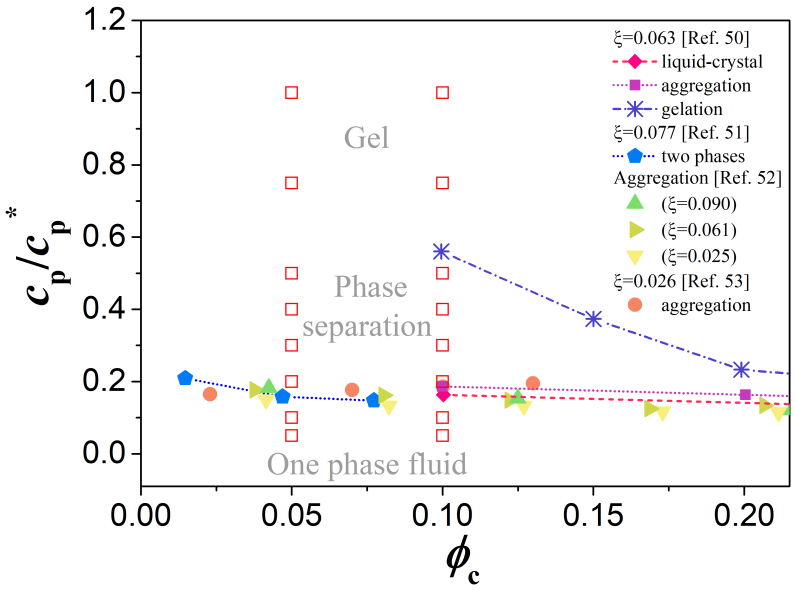

Figure 1: State diagram of colloid-polymer mixtures with small size ratio, ξ. Data were taken from the following experimental contributions: [50] (diamonds, squares, stars), [51] (pentagons), [52] (triangles), and [53] (circles). Lines are a guide for the eye to identify different thermodynamic phases, namely one phase fluid, fluid-crystal coexistence, fluid-fluid phase coexistence, aggregation of particles and gel. The experimental states studied in this work are also displayed (open squares). Error bars are smaller than the symbols.

the VLc criterion, one gets that the onset of the phase separation for short-range attractions starts at $c_p/c_p^* \sim 1.66$. As we will see further below, this is a considerably higher value than the one obtained in both experiments and computer simulations. However, Eq. 5 provides a qualitative support of the relation between B_2 and c_p/c_p^*, being the latter that consistently allows us to describe the connection between cluster morphology and the extended law of corresponding state.

3. Results and Discussions

3.1. Colloid-polymer state diagram: thermodynamic identification of clusters

Recently, we have reported on the structure of a colloid-polymer mixture similar to that investigated here, for which we found that colloids mainly interact through a short-range depletion attraction [31].

Results of previous studies [50, 51, 52, 53] on the state diagram of colloid-polymer mixtures with small values of ξ are summarized in Fig. 1, in which we additionally included the experimental states explored in this work (open squares); sample preparation is summarized in section 2.1. This allows us to locate the thermodynamic regions in which our study has been performed. The diagram reports the observed states in the parameter space (ϕ_c, c_p/c_p^*) with ϕ_c to be the colloid volume fraction. Even though the

experimental criteria used by different authors can be slightly different, one can evince that at low polymer concentrations, $c_p/c_p^* < 0.2$, the mixture is in a liquid state. On the other hand, at $c_p/c_p^* \gtrsim 0.2$ phase separation/aggregation is observed for the smallest ξ and ϕ_c values. For larger values of c_p/c_p^*, a gel network, i.e., a mechanically stable space spanning network of aggregated particles, is formed [4]; the onset of gelation shifts to smaller values of c_p/c_p^* with increasing ϕ_c. Summarizing, for $\phi_c < 0.20$ the mixture experiences transitions between different thermodynamic states, namely, a one phase fluid at low polymer concentrations, heterogeneous states at intermediate c_p values and non-equilibrium or gel-like states at high polymer concentrations. This scenario appears almost independently of ξ provided it is smaller than approximately 0.1. Our experiments were carried out at $\phi_c = 0.05$ and 0.10 for several values of c_p/c_p^* and ξ (< 0.1). In this way, we systematically explored and studied the connection between cluster structure and attraction strength and range in the different thermodynamic states of the mixtures.

Figure 2(A) presents the state diagram of cluster morphologies of the experimental system in the (c_p/c_p^*, ξ) space. The geometric shapes of clusters observed were obtained by confocal microscopy as described in section 2.2. Note that two particles are considered to form a bond and thus belong to the same cluster when the distance between their centers is smaller than $2R + 2r_g$, i.e. when they lie within the range of the attractive interaction induced by depletion forces. We have reported data for the samples with $\phi_c = 0.10$. The same behavior was observed for $\phi_c = 0.05$ (data not shown). The solid line in Figure 2(A) corresponds to the value of c_p/c_p^* at which the gas-liquid phase separation occurs in Monte Carlo simulations, as discussed in section 2.4 and in the Supplementary Information. We have identified a region where colloidal particles are dispersed forming a one phase colloidal fluid and another one where particles form clusters. The boundary between these two regions is close to the gas-liquid phase separation line determined from MC simulations and predicted by FVT [48]. This indicates that the simulated system qualitatively reproduces the phase behavior of the experimental system.

Figs. 2(B) and (C) show snapshots of representative experimental samples for $\xi = 0.075$ and 0.011, respectively. From the snapshots, one can see that the morphology of clusters does depend on the attraction range. Longer attraction ranges produce more compact clusters (Fig. 2(B)) for $c_p = 0.30\, c_p^*$ and $0.50\, c_p^*$. More elongated clusters are instead formed for shorter attraction ranges, as shown in Fig. 2(C) for corresponding values of c_p/c_p^*. In addition, the system with the shortest attractive range forms colloidal aggregates at smaller polymer concentrations. A more quantitative criterion based on the average number of neighbors $\langle n \rangle$, explained in section 2.3, was used to distinguish the regions of compact and elongated clusters shown in Fig. 2. Additional analysis of the cluster morphology based on the determination of the fractal dimension of clusters composed of up to 100 particles is reported in more detail further below.

3.2. Cluster size distribution

The experimental samples present a distribution of cluster sizes which can be associated with specific structural and dynamical arrangements, i.e., particle bonds are continuously formed and broken [54]. Figure 3 shows the cluster size distribution, $P(s)$, as a function of the number of particles forming a cluster, s, for different c_p/c_p^*

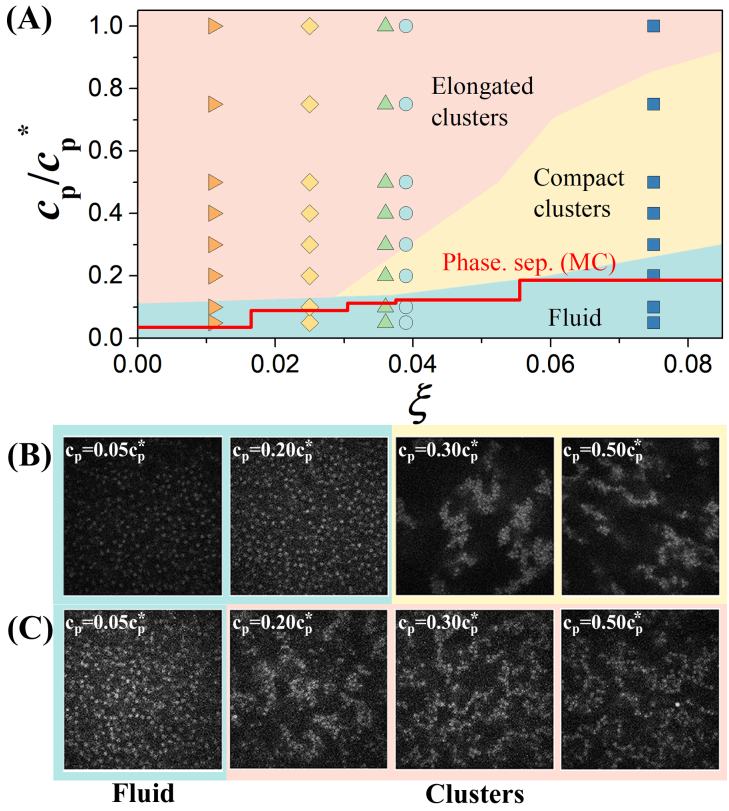

Figure 2: (A) Phase diagram of the investigated colloid-polymer mixture for small size ratios, ξ and $\phi_c = 0.1$. We identify two states: one phase fluid and clustered structures. The latter are composed of either compact or elongated clusters, see, e.g., section 2.3. Solid line is the phase separation boundary for a colloidal dispersion with $\phi_c = 0.1$ obtained from Monte Carlo simulations; a polydisperse system of particles interacting through an Asakura-Oosawa potential was considered, see, e.g., section 2.4 and the Supplementary Information. Experimental snapshots for (B) $\xi = 0.075$ and (C) $\xi = 0.011$ at different polymer concentrations, as indicated.

values and attraction ranges ξ. This distribution presents an exponential decay making more relevant the population of small clusters. To avoid that bias we report $sP(s)$ [55]. For the lowest values of c_p/c_p^*, most of the particles are forming small clusters, as can be seen from the distribution in panel (A). As the polymer concentration increases, larger clusters appear due to the strong attraction between particles. However, colloid-polymer systems with the smallest attraction ranges, ξ =0.011 and 0.025, do not present clusters with much more than 100 particles for any polymer concentration. This confirms the qualitative indication obtained from the snapshots in Figure 2C and is in agreement with a more elongated cluster morphology. We note that this result could be slightly influenced by the fact that the error associated with particle positions is close to the bonding distance we have defined, see section 2.3.

At the percolation threshold, one expects that the cluster size distribution follows the power law $P(s) \propto s^{-2.2}$, as it occurs in other systems with short-ranged attractions, see, e.g., Ref. [56]. The exponent in this power law is characteristic of the process known as random percolation. Such scaling law is shown as dashed lines in panels (B)-(D) of Figure 3. If a system crosses the percolation threshold, several points are expected to lie above the power-law line. As it can be seen in the systems with ξ larger than 0.25, several points lie above the percolation line thus indicating the presence of a percolating cluster coexisting with small clusters. Note that this could also indicate the formation of a gel state, as long as the percolating cluster is mechanically stable [56]. In systems with competing interactions, the size distribution presents a secondary peak at about 20 particles which indicates a preferential size for clusters. Here, we do not find any clear indication of such peak, supporting our assumption that the main driving force in the colloid-polymer mixtures is the short-ranged attraction.

3.3. Cluster morphology

We now focus on the morphology of clusters for the extreme cases, namely, ξ = 0.075 and 0.011. In Fig. 4, the radius of gyration of clusters made of s-particles, $R_g(s)$, is displayed; $R_g(s)$ is defined in section 2.2. The top graph shows the results for small clusters, $2 \leq s \leq 10$, while the bottom one those for large clusters, $10 < s \leq 100$. We should point out that a distinction between small and large clusters was made because $R_g(s)$ cannot be properly fitted with a single power-law dependence: instead, two power-law dependencies with different fractal exponents need to be used to correctly reproduce the entire experimental trend, which exhibits a clear crossover at $s = 10$ (Fig. S4 of the Supplementary Information), in good agreement with previous simulation predictions [30]. The determination of a fractal dimension for small clusters ($s < 10$) may not be entirely meaningful. However, to be consistent with previous contributions [30, 57] and to be able to compare with those results, we have decided to still extract a nominal fractal dimension from the slope of R_g for small aggregates. For large clusters, we additionally decided to limit the plot to s = 100 particles, since only a few larger clusters are present which have no statistical significance. Moreover, in this way we exclude from the analysis the gel network backbone in gelled samples. Fig. 4 also reports a line indicating the power-law $R_g \propto s^{1/2}$ that corresponds to a cluster fractal dimension of 2. This provides a reference for comparison with the fractal dimension of clusters in the experimental samples.

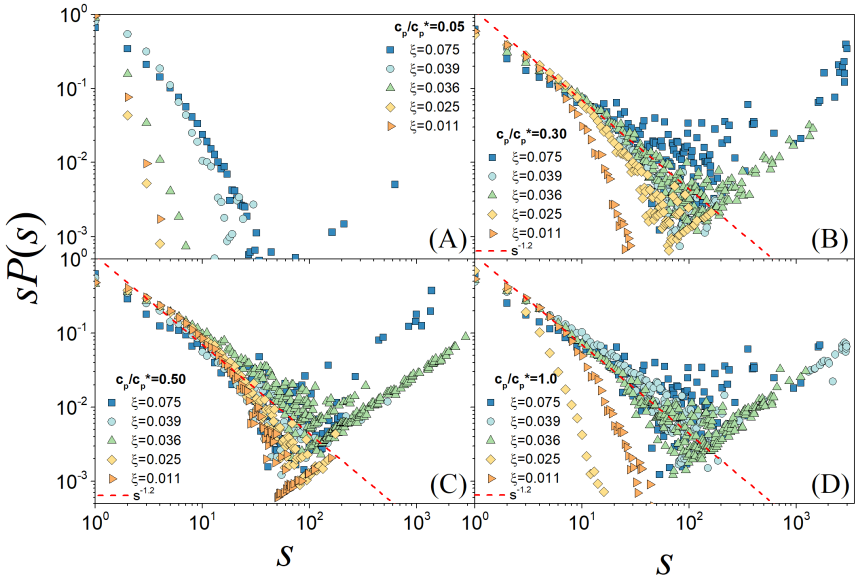

Figure 3: Cluster size distribution of colloid-polymer mixtures with $\phi_c = 0.10$ and different polymer concentrations, c_p/c_p^*. (A) c_p/c_p^* = 0.05, (B) 0.30, (C) 0.50 and (D) 1.0 and ξ values (as indicated).

In a previous contribution [30], we pointed out that small clusters in simulated dispersions of attractive colloids are not much sensitive to the thermodynamic state of the system. Panels (A) and (B) of Fig. 4, which correspond to $\xi = 0.75$ and $\xi = 0.011$, respectively, show that for the experiments reported here the morphology of small clusters seems to change when the state of the system changes from the one phase fluid to a clustered structure (either a cluster fluid or gel). In particular, the slope slightly increases when passing from the fluid to the clustered state, indicative of a moderate decrease in the fractal dimension. For the larger clusters instead the slopes are comparable for most samples for both values of ξ (Fig. 4(C) and (D)). This is particularly true within the clustered region, where thus the morphology changes only slightly while the attraction amplitude changes of several k_BT from $c_p/c_p^* = 0.3$ to 1.0, in agreement with previous results reported in Ref. [12].

3.4. Fractal dimension and the extended law of corresponding states

According to the extended law of corresponding states, the properties of two systems are expected to be the same when they are compared at the same reduced density and second virial coefficient (B_2^*). In previous contributions [30], we showed that the cluster morphology, in particular the fractal dimension d_f, depends on B_2^* for simulated attractive colloidal model systems interacting through a square-well potential. Moreover, we found that sparse literature data on experimental colloid-polymer mixtures present a similar dependence when replacing B_2^* with c_p/c_p^*. Here, supported by predictions of FVT [35]] that indicate that B_2^* is indeed determined by c_p/c_p^* in the limit of short range attractions (see previous section), we systematically investigate the relation

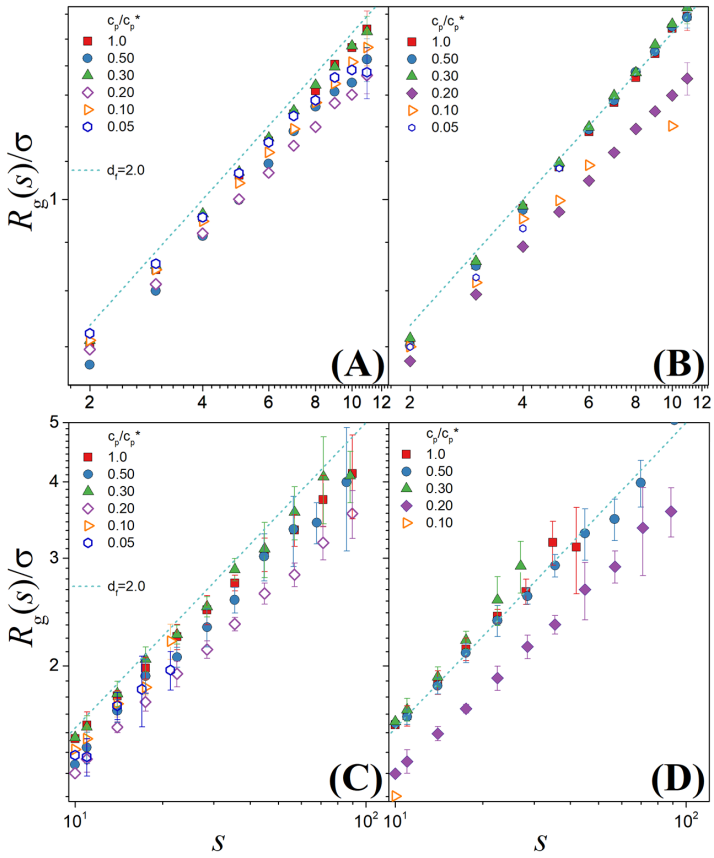

Figure 4: Radius of gyration $R_g(s)$ of colloid-polymer systems with $\xi = 0.75$ and $\xi = 0.011$ for different polymer concentrations. Systems in a clustered state are represented by an empty (solid) symbol. Top row shows data for small clusters and bottom row for large clusters. (A) and (B) correspond to $\xi = 0.075$ and (C) and (D) to $\xi = 0.011$. Error bars indicate one standard deviation of uncertainty.

between d_f and c_p/c_p^* in experimental colloid-polymer mixtures for an extensive set of polymer-colloid size ratios. We chose to present d_f vs. c_p/c_p^* instead of B_2^* since the FVT relation might not be quantitatively accurate, as discussed in Sec.2.5. In addition, we show that simulation data for a system interacting with the AO potential, which better approximates experimental interactions, also confirm the relation between d_f and ϕ_p (B_2^*).

In order to compare experiments and simulations, the values of c_p/c_p^* and ϕ_p were normalized with the respective critical values for phase separation. In the case of simulations, this value was directly determined for the different values of ξ, as explained in section 2.4. For the experiments, the critical value was estimated as the value of c_p/c_p^* at which gelation is observed. Indeed, for short-range attractions gelation can be described as the result of arrested spinodal decomposition [4] and therefore the onset of gelation corresponds to the onset of spinodal decomposition. Additionally, in the

limit of small ξ values, the binodal and spinodal lines are very close, and therefore the gelation line is a reasonable estimate of the binodal. The location of the gelation line was determined in previous work [31]. For simplicity, we use in what follows c_p/c_p^c to indicate the normalized values of both experimental and simulation data.
Figure 5 reports the fractal dimension of small (A) and large (B) clusters obtained in experiments and simulations as a function of c_p/c_p^c, for different values of the size ratio ξ.
Plot (A) contains the information for small clusters and Plot (B) that for large clusters. For both small and large clusters, results of experiments and simulations for different values of ξ are comparable, confirming that cluster morphology is determined by c_p/c_p^*, and consequently B_2^*. We remark that the observed collapse of experimental data for different value of ξ over a broad range of c_p/c_p^* values was not reported before. Note additionally that the collapse of the experimental data induced by plotting d_f vs. c_p/c_p^* is evidenced in particular by the values of d_f close to the fluid-gel boundary, which present the most pronounced dependence on c_p: as shown in the Supplementary Information (Fig. S5), those data are far from collapsing when plotted against c_p for each sample. We should remark that experiments and simulations represent different regions of the state diagram: while experimental data lie within the metastable region, simulation data lie in the fluid phase.

The values of d_f of the small clusters for experimental samples in the fluid phase were not statistically significant and were thus not included in Panel (A). At the same time, simulation data are not available inside the metastable region predicted by the Asakura-Oosawa interaction. The different location of experimental and simulation data in the state diagram explains the different trends observed as a function of c_p/c_p^*: in the simulations d_f increases while c_p/c_p^* increases, which indicates formation of more compact structures as an effect of the density fluctuations induced by phase separation. In the experiments, instead, d_f decreases in the metastable region, as observed before [58], indicating the formation of progressively more elongated clusters. The elongated small clusters might be the result of more rigid bonds associated with the stronger attraction, which reduces the ability of bond reorientation to form more compact aggregates. Note that the data for small clusters corresponding to the large value of $\xi = 0.075$ slightly deviate from the other data in the meta-stable region (also in agreement with the state diagram of Fig. 2), suggesting that the description of cluster morphology in terms of c_p/c_p^* and thus B_2^* starts to be less accurate when the range of attraction becomes larger. Large clusters in experiments do not seem to indicate a significant dependence on c_p/c_p^*. Conversely, large clusters in simulations show a trend similar to that observed for small clusters, even though with larger statistical fluctuations. As previously observed, the fractal dimension of the large clusters is bigger than that of small clusters. Results of experiments and simulations are consistent with previous findings [30].

3.5. Conclusions and perspectives

Combining experiments on model colloid-polymer mixtures and simulations of particles interacting through the Asakura-Oosawa potential, we demonstrated that cluster morphology in colloidal systems with short-range attractions is determined by c_p/c_p^*

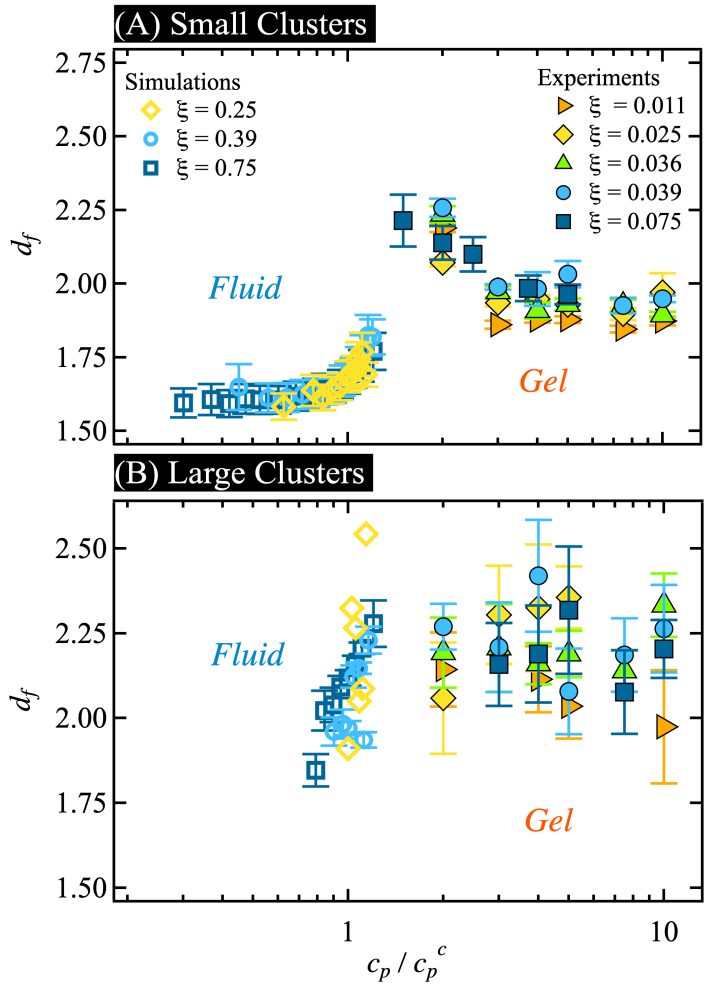

Figure 5: Fractal dimension of (A) small and (B) large clusters, according to the distinction employed in Fig. 4, as a function of c_p/c_p^c, for different values of the size ratio ξ, as indicated. Closed symbols correspond to results of confocal microscopy experiments, while open symbols to results of Monte Carlo simulations. Error bars indicate one standard deviation of uncertainty.

and therefore by the reduced second virial coefficient B_2^*. This was confirmed by examining the fractal dimension of clusters in systems with different (short) attraction ranges and in different thermodynamic states, namely, equilibrium one phase fluid states and non-equilibrium gel-like states. In addition, the analysis of the cluster morphology made evident the presence of distinct populations of small and large clusters characterized by different fractal dimensions (smaller for the smaller clusters) and dependent on B_2^*. In the fluid states, for small values of B_2^*, the small clusters show a poor dependence on B_2^* and suddenly become more compact while approaching the phase separation boundary, and so the large clusters. The experimental system allowed us to additionally investigate the much less explored metastable region, in which the colloid-polymer mixture typically forms gel states. In this region, the cluster morphology is generally poorly dependent on the second virial coefficient, with the small clusters showing a moderate decrease with increasing $c_\mathrm{p}/c_\mathrm{p}^*$.
Our findings, by revealing the control parameter that drives cluster morphology in attractive colloidal dispersions, open up the way to a programmable design of heterogeneous structures with desired cluster morphologies, with potential applications in photonics [59], biology [60], foodstuff [61], transport behavior in tunable fractal-like structures [62], among others. Furthermore, our results have experimentally confirmed the general validity of the extended law of corresponding states to describe not only macroscopic or thermodynamic properties, but also local ones, such as the degree of compaction of the resulting clusters and, mainly, to become the main driving force behind the mechanisms of aggregation in liquids of clusters made up of sticky-like colloids. Additional studies on different types of colloidal systems, namely dispersions with highly directional interactions, should be performed to test the limits of applicability of our results.

Author Contributions

F. Soto-Bustamante: Investigation, Validation, Formal analysis, Visualization, Writing - review & editing. **N. E. Valadez-Perez**: Investigation, Validation, Formal analysis, Visualization, Writing - original draft. **Y. Liu** Supervision, Conceptualization, Writing - review & editing. **R. Castañeda-Priego** Supervision, Resources, Conceptualization, Funding acquisition, Writing - original draft. **M. Laurati** Supervision, Resources, Conceptualization, Funding acquisition, Writing - review & editing.

Declaration of Competing Interests

The authors declare that they have no known competing financial interests or personal relationships that could have appeared to influence the work reported in this paper.

Acknowledgments

We acknowledge financial support from the project "A1-S-9098" funded by Conacyt within the call "Convocatoria de Investigación Básica 2017-2018" and from "Consorzio per lo Sviluppo dei Sistemi a Grande Interfase" (CSGI). R. C-P. also thanks

financial support provided by Conacyt (Grants No. 237425 and 287067) and the Marcos Moshinsky Foundation. N.E.V.P. thanks the financial support provided by the Autonomous University of Chiapas (Grant No. 01/FYM/RPR/278/20). Certain commercial equipment, instruments, or materials (or suppliers, or software, ...) are identified in this paper to foster understanding. Such identification does not imply recommendation or endorsement by the National Institute of Standards and Technology, nor does it imply that the materials or equipment identified are necessarily the best available for the purpose.

References

[1] H. N. Lekkerkerker, W. C. K. Poon, P. N. Pusey, A. Stroobants, P. . Warren, Phase behaviour of colloid + polymer mixtures, Europhys. Lett. 20 (6) (1992) 559.

[2] S. M. Ilett, A. Orrock, W. C. K. Poon, P. Pusey, Phase behavior of a model colloid-polymer mixture, Phys. Rev. E 51 (2) (1995) 1344.

[3] W. C. K. Poon, The physics of a model colloid–polymer mixture, J. Phys. Condens. Matter 14 (33) (2002) R859.

[4] P. J. Lu, E. Zaccarelli, F. Ciulla, A. B. Schofield, F. Sciortino, D. A. Weitz, Gelation of particles with short-range attraction, Nature 453 (7194) (2008) 499–503.

[5] J. Bentley, G. P. A. Turner, Introduction to paint chemistry and principles of paint technology, CRC Press, 1997.

[6] R. Mezzenga, P. Schurtenberger, A. Burbidge, M. Michel, Understanding foods as soft materials, Nat. Mater. 4 (10) (2005) 729–740.

[7] E. Dickinson, M. E. Leser (Eds.), Food Colloids, Special Publications, The Royal Society of Chemistry, 2007. doi:10.1039/9781847557698.
URL http://dx.doi.org/10.1039/9781847557698

[8] G. Tiwari, R. Tiwari, B. Sriwastawa, L. Bhati, S. Pandey, P. Pandey, S. K. Bannerjee, Drug delivery systems: An updated review, Int. J. Pharm. Investig. 2 (1) (2012) 2.

[9] W. C. K. Poon, Colloids as big atoms, Science 304 (5672) (2004) 830–831.

[10] V. N. Manoharan, Colloidal matter: Packing, geometry, and entropy, Science 349 (6251) (2015).

[11] P. J. Lu, J. C. Conrad, H. M. Wyss, A. B. Schofield, D. A. Weitz, Fluids of clusters in attractive colloids, Phys. Rev. Lett. 96 (2) (2006) 028306.

[12] T. Ohtsuka, C. P. Royall, H. Tanaka, Local structure and dynamics in colloidal fluids and gels, Europhys. Lett. 84 (4) (2008) 46002.

[13] G. Meng, N. Arkus, M. P. Brenner, V. N. Manoharan, The free-energy landscape of clusters of attractive hard spheres, Science 327 (5965) (2010) 560–563.

[14] R. W. Perry, G. Meng, T. G. Dimiduk, J. Fung, V. N. Manoharan, Real-space studies of the structure and dynamics of self-assembled colloidal clusters, Faraday Disc. 159 (1) (2012) 211–234.

[15] A. Dinsmore, D. Weitz, Direct imaging of three-dimensional structure and topology of colloidal gels, J. Phys.: Condens. Matter 14 (33) (2002) 7581.

[16] P. D. Godfrin, N. E. Valadez-Pérez, R. Castaneda-Priego, N. J. Wagner, Y. Liu, Generalized phase behavior of cluster formation in colloidal dispersions with competing interactions, Soft matter 10 (28) (2014) 5061–5071.

[17] P. D. Godfrin, S. D. Hudson, K. Hong, L. Porcar, P. Falus, N. J. Wagner, Y. Liu, Short-time glassy dynamics in viscous protein solutions with competing interactions, Phys. Rev. Lett. 115 (22) (2015) 228302.

[18] H. Tsurusawa, S. Arai, H. Tanaka, A unique route of colloidal phase separation yields stress-free gels, Sci. Adv. 6 (41) (2020) eabb8107.

[19] C. P. Royall, S. R. Williams, T. Ohtsuka, H. Tanaka, Direct observation of a local structural mechanism for dynamic arrest, Nat. Mater. 7 (7) (2008) 556–561.

[20] S. J. Khan, O. Weaver, C. Sorensen, A. Chakrabarti, Nucleation in short-range attractive colloids: ordering and symmetry of clusters, Langmuir 28 (46) (2012) 16015–16021.

[21] N. Kovalchuk, V. Starov, P. Langston, N. Hilal, Formation of stable clusters in colloidal suspensions, Adv. Colloid Interface Sci. 147 (2009) 144–154.

[22] W. C. K. Poon, A. D. Pirie, P. N. Pusey, Gelation in colloid–polymer mixtures, Faraday Discuss. 101 (1995) 65–76. doi:10.1039/FD9950100065.
URL http://dx.doi.org/10.1039/FD9950100065

[23] M. Lattuada, H. Wu, A. Hasmy, M. Morbidelli, Estimation of fractal dimension in colloidal gels, Langmuir 19 (15) (2003) 6312–6316.

[24] R. Sanchez, P. Bartlett, Equilibrium cluster formation and gelation, J. Phys.: Condens. Matt. 17 (45) (2005) S3551.

[25] M. Lin, H. Lindsay, D. Weitz, R. Ball, R. Klein, P. Meakin, Universal reaction-limited colloid aggregation, Phys. Rev. A 41 (4) (1990) 2005.

[26] E. A. Guggenheim, The principle of corresponding states, J. Chem. Phys. 13 (7) (1945) 253–261.

[27] M. G. Noro, D. Frenkel, Extended corresponding-states behavior for particles with variable range attractions, J. Chem. Phys. 113 (8) (2000) 2941–2944.

[28] G. A. Vliegenthart, H. N. W. Lekkerkerker, Predicting the gas–liquid critical point from the second virial coefficient, The Journal of Chemical Physics 112 (12) (2000) 5364–5369. arXiv:https://doi.org/10.1063/1.481106, doi:10.1063/1.481106.
URL https://doi.org/10.1063/1.481106

[29] N. E. Valadez-Pérez, A. L. Benavides, E. Scholl-Paschinger, R. Castañeda Priego, Phase behavior of colloids and proteins in aqueous suspensions: Theory and computer simulations, J. Chem. Phys. 137 (8) (2012).

[30] N. E. Valadez-Pérez, Y. Liu, R. Castañeda-Priego, Reversible aggregation and colloidal cluster morphology: the importance of the extended law of corresponding states, Phys. Rev. Lett. 120 (24) (2018) 248004.

[31] F. Soto-Bustamante, N. E. Valádez-Pérez, R. Castañeda-Priego, M. Laurati, Potential-invariant network structures in asakura–oosawa mixtures with very short attraction range, J. Chem. Phys. 155 (3) (2021) 034903.

[32] M. Dijkstra, J. M. Brader, R. Evans, Phase behaviour and structure of model colloid-polymer mixtures, J. Phys.: Condens. Matter 11 (50) (1999) 10079.
URL http://stacks.iop.org/0953-8984/11/i=50/a=304

[33] S. Asakura, F. Oosawa, On interaction between two bodies immersed in a solution of macromolecules, J. Chem. Phys. 22 (7) (1954) 1255–1256.

[34] N. M. de los Santos-López, G. Pérez-Ángel, J. M. Méndez-Alcaraz, R. Castañeda-Priego, Competing interactions in the depletion forces of ternary colloidal mixtures, J. Chem. Phys. 155 (2) (2021) 024901. arXiv:https://doi.org/10.1063/5.0052369, doi:10.1063/5.0052369.
URL https://doi.org/10.1063/5.0052369

[35] R. Tuinier, M. S. Feenstra, Second Virial Coefficient at the Critical Point in a Fluid of Colloidal Spheres Plus Depletants, Langmuir 30 (44) (2014) 13121–13124. doi:10.1021/la5023856.
URL https://doi.org/10.1021/la5023856

[36] G. Berry, Thermodynamic and conformational properties of polystyrene. i. light-scattering studies on dilute solutions of linear polystyrenes, J. Chem. Phys. 44 (12) (1966) 4550–4564.

[37] C. P. Royall, M. E. Leunissen, A.-P. Hynninen, M. Dijkstra, A. van Blaaderen, Re-entrant melting and freezing in a model system of charged colloids, J. Chem. Phys. 124 (24) (2006) 244706.

[38] C. P. Royall, W. C. K. Poon, E. R. Weeks, In search of colloidal hard spheres, Soft Matter 9 (2013) 17–27. doi:10.1039/C2SM26245B.
URL http://dx.doi.org/10.1039/C2SM26245B

[39] M. Kohl, R. F. Capellmann, M. Laurati, S. U. Egelhaaf, M. Schmiedeberg, Directed percolation identified as equilibrium pre-transition towards non-equilibrium arrested gel states, Nat. Commun. 7 (2016) 11817.

[40] J. C. Crocker, D. G. Grier, Methods of digital video microscopy for colloidal studies, J. Colloid Interface Sci. 179 (1) (1996) 298–310.

[41] E. M. Sevick, P. A. Monson, J. M. Ottino, Monte carlo calculations of cluster statistics in continuum models of composite morphology, J. Chem. Phys. 88 (2) (1988) 1198–1206.

[42] P. D. Godfrin, R. Castaneda-Priego, Y. Liu, N. J. Wagner, Intermediate range order and structure in colloidal dispersions with competing interactions, J. Chem. Phys. 139 (15) (2013) –.

[43] A. Gast, C. Hall, W. Russel, Polymer-induced phase separations in nonaqueous colloidal suspensions, J. Colloid Interface Sci. 96 (1) (1983) 251–267. doi:https://doi.org/10.1016/0021-9797(83)90027-9.
URL https://www.sciencedirect.com/science/article/pii/0021979783900279

[44] K. Binder, P. Virnau, A. Statt, Perspective: The asakura oosawa model: A colloid prototype for bulk and interfacial phase behavior, J. Chem. Phys. 141 (14) (2014) 140901. arXiv:https://doi.org/10.1063/1.4896943, doi:10.1063/1.4896943.
URL https://doi.org/10.1063/1.4896943

[45] D. G. A. L. Aarts, R. Tuinier, H. N. W. Lekkerkerker, Phase behaviour of mixtures of colloidal spheres and excluded-volume polymer chains, J. Phys.: Condens. Matter 14 (33) (2002) 7551–7561. doi:10.1088/0953-8984/14/33/301.
URL https://doi.org/10.1088%2F0953-8984%2F14%2F33%2F301

[46] G. J. Fleer, A. M. Skvortsov, R. Tuinier, Macromol. theory simul. 5/2007, Macromolecular Theory and Simulations 16 (5) (2007) 493–493. arXiv:https://onlinelibrary.wiley.com/doi/pdf/10.1002/mats.200790008, doi:https://doi.org/10.1002/mats.200790008.
URL https://onlinelibrary.wiley.com/doi/abs/10.1002/mats.200790008

[47] R. Tuinier, P. A. Smith, W. C. K. Poon, S. U. Egelhaaf, D. G. A. L. Aarts, H. N. W. Lekkerkerker, G. J. Fleer, Phase diagram for a mixture of colloids and polymers with equal size, EPL (Europhysics Letters) 82 (6) (2008) 68002. doi:10.1209/0295-5075/82/68002.
URL https://doi.org/10.1209/0295-5075/82/68002

[48] G. J. Fleer, R. Tuinier, Analytical phase diagrams for colloids and non-adsorbing polymer, Advances in Colloid and Interface Science 143 (1) (2008) 1–47. doi:https://doi.org/10.1016/j.cis.2008.07.001.
URL https://www.sciencedirect.com/science/article/pii/S0001868608001127

[49] M. Fuchs, K. S. Schweizer, Macromolecular theory of solvation and structure in mixtures of colloids and polymers, Phys. Rev. E 64 (2001) 021514. doi:10.1103/PhysRevE.64.021514.
URL https://link.aps.org/doi/10.1103/PhysRevE.64.021514

[50] W. C. K. Poon, L. Starrs, S. Meeker, A. Moussaid, R. M. Evans, P. Pusey, M. Robins, Delayed sedimentation of transient gels in colloid–polymer mixtures: dark-field observation, rheology and dynamic light scattering studies, Faraday Disc. 112 (1999) 143–154.

[51] E. H. de Hoog, W. K. Kegel, A. van Blaaderen, H. N. Lekkerkerker, Direct observation of crystallization and aggregation in a phase-separating colloid-polymer suspension, Phys. Rev. E 64 (2) (2001) 021407.

[52] S. Shah, Y.-L. Chen, K. Schweizer, C. Zukoski, Viscoelasticity and rheology of depletion flocculated gels and fluids, J. Chem. Phys. 119 (16) (2003) 8747–8760.

[53] H. Sedgwick, S. U. Egelhaaf, W. C. K. Poon, Clusters and gels in systems of sticky particles, J. Phys.: Condens. Matter 16 (42) (2004) S4913.

[54] M. Rottereau, J. C. Gimel, T. Nicolai, D. Durand, Monte carlo simulation of particle aggregation and gelation: I. growth, structure and size distribution of the clusters, Europhys. J. E 15 (2) (2004) 133–140. doi:10.1140/epje/i2004-10044-x.
URL https://doi.org/10.1140/epje/i2004-10044-x

[55] L. V. Woodcock, Percolation transitions in the hard-sphere fluid, AIChE J. 58 (5) (2012) 1610–1618. arXiv:https://aiche.onlinelibrary.wiley.com/doi/pdf/10.1002/aic.12666, doi:https://doi.org/10.1002/aic.12666.
URL https://aiche.onlinelibrary.wiley.com/doi/abs/10.1002/aic.12666

[56] N. E. Valadez-Pérez, R. Castañeda-Priego, Y. Liu, Percolation in colloidal systems with competing interactions: the role of long-range repulsion, Rsc Adv. 3 (47) (2013) 25110–25119.

[57] D. Banerjee, B. A. Lindquist, R. B. Jadrich, T. M. Truskett, Assembly of particle strings via isotropic potentials, The Journal of Chemical Physics 150 (12) (2019) 124903. arXiv:https://doi.org/10.1063/1.5088604, doi:10.1063/1.5088604.
URL https://doi.org/10.1063/1.5088604

[58] C. J. Dibble, M. Kogan, M. J. Solomon, Structure and dynamics of colloidal depletion gels: Coincidence of transitions and heterogeneity, Phys. Rev. E 74 (2006) 041403. doi:10.1103/PhysRevE.74.041403.
URL https://link.aps.org/doi/10.1103/PhysRevE.74.041403

[59] Z. Cai, Z. Li, S. Ravaine, M. He, Y. Song, Y. Yin, H. Zheng, J. Teng, A. Zhang, From colloidal particles to photonic crystals: advances in self-assembly and their emerging applications, Chem. Soc. Rev. 50 (2021) 5898–5951. doi:10.1039/D0CS00706D.
URL http://dx.doi.org/10.1039/D0CS00706D

[60] S. K. Nair, S. Basu, B. Sen, M.-H. Lin, A. N. Kumar, Y. Yuan, P. J. Cullen, D. Sarkar, Colloidal gels with tunable mechanomorphology regulate endothelial morphogenesis, Sci. Rep. 9 (1) (2019) 1–17.

[61] Y. Cao, R. Mezzenga, Design principles of food gels, Nat. Food 1 (2) (2020) 106–118.

[62] R. Perdomo-Perez, E. Lazaro-Lazaro, L. F. Elizondo-Aguilera, T. Voigtmann, R. Castañeda-Priego, to be submitted.